OPEN

SWEPT-SOURCE OPTICAL COHERENCE TOMOGRAPHY ANGIOGRAPHY IN SMALL CHOROIDAL MELANOMAS AND CHOROIDAL NEVI

EUGENIA CUSTO GREIG, BA,*† NORA V. LAVER, MD,* LUISA S.M. MENDONCA, MD,*‡ EMILY S. LEVINE, BS,* CAROLINE R. BAUMAL,* NADIA K. WAHEED, MD, MPH,* JAY S. DUKER, MD*

Purpose: To evaluate the use of swept-source optical coherence tomography angiography to detect distinct vascular features in small choroidal melanomas and choroidal nevi.

Methods: Patients with a choroidal nevus or a treatment-naïve choroidal melanoma were imaged with color fundus photography, ultrasound, and swept-source optical coherence tomography angiography (12 × 12 mm). High-risk features including overlying fluid, orange pigment, shaggy photoreceptors, acoustic hollowness, depth >2 mm, and basal diameter >5 mm were assessed. Optical coherence tomography angiography vascular markers included: choroidal vessel visualization, choroidal vessel depth, and choriocapillaris flow signal, assessed qualitatively by comparison with surrounding, unaffected choriocapillaris.

Results: Twenty-nine lesions were included in this study, seven flat choroidal nevi, 17 elevated choroidal nevi, and 5 choroidal melanomas. Distinct vascular patterns were noted between flat nevi, elevated nevi, and small choroidal melanomas. Choroidal melanomas displayed two types of vasculature: "nevus-like" vasculature with straight parallel vessels and complex vasculature with vascular loops and crosslinking. Visualized choroidal vessels were significantly deeper in melanomas (110 μm) than elevated (84 μm) or flat nevi (70 μm). In a size-matched subanalysis of 5 elevated choroidal nevi and 5 choroidal melanomas, choroidal melanomas had increased mean choroidal vessel depth (P = 0.015), deepest choroidal vessel visualized (P = 0.034), and presence of a deep choroidal vessel >155 μm (P = 0.048).

Conclusion: Swept-source optical coherence tomography angiography may detect distinct vascular features in choroidal nevi and small choroidal melanomas.

RETINA 41:1182–1192, 2021

Early detection of choroidal melanoma is a key to successful treatment and improved survival.[1] Distinguishing small choroidal melanomas from benign nevi is challenging, but essential for prompt and accurate treatment.[2] Currently, differentiation between choroidal nevi and small choroidal melanomas relies largely on high-risk feature identification and serial examination. Identification of additional features that accurately identify malignancy and predict future transformation to malignancy would be of significant value.

Histologic studies comparing melanoma and nevus vasculature reveal clear differences. The internal vasculature of nevi consists of straight, parallel vessels, a pattern that resembles normal choroidal vasculature. By contrast, choroidal melanomas have complex vascular patterns with vessel cross-linking and loops.[3] A subset of melanomas with benign "nevus-like" architecture also exists.[4] Given vascular differences and similarities across lesion types, pathologists postulate a spectrum of vascular progression between choroidal nevi and melanomas.[4]

Developments in optical coherence tomography angiography (OCTA) technology permit improved assessment of deep retinal microvasculature in vivo. Previous studies using spectral-domain OCTA (SD-OCTA) to assess the vasculature of choroidal melanomas and nevi have been limited by signal depth penetration.[5–7] Newer swept-source OCTA

(SS-OCTA) technology uses a tunable laser with a wavelength of ~1060 nm.[8] Increased laser wavelength and scan speeds allow for increased penetration through the retinal pigment epithelium (RPE) and larger scan areas, making SS-OCTA particularly useful for the assessment of choroidal lesions.[9]

Two recent studies revealed successful vascular evaluation of choroidal nevi and melanomas using SS-OCTA. The first study by Ali et al[10] focused on the use of structural reverse flow to identify choroidal nevi. The second study by Pellegrini et al[11] showed the ability of SS-OCTA to identify tumor microvasculature in choroidal melanomas. Although these studies showed the use of SS-OCTA for choroidal lesion visualization, they did not compare melanomas and nevi, nor did they elucidate vascular patterns found in each. The current study compares the vascular patterns of choroidal nevi and melanomas in search of vascular features that might aid in lesion differentiation.

Methods

Subjects

This was a cross-sectional study of patients with a diagnosis of choroidal nevus or treatment-naïve choroidal melanoma seen at the New England Eye Center from September 2019 to May 2020. The study was approved by the Institutional Review Board at Tufts Medical Center and adhered to the principles of the Declaration of Helsinki and the Health Insurance Portability and Accountability act of 1996.

The inclusion criteria comprised a diagnosis of choroidal nevus or treatment-naïve choroidal melanoma as determined by the institution's ocular oncologist (JSD). Clinical and imaging features obtained on color fundus photography, ultrasound (US), and optical coherence tomography (OCT) were used for diagnosis. Lesions did not undergo pathologic confirmation of the clinical diagnosis. Choroidal nevi were subclassified as elevated or flat. Flat nevi had no elevation on clinical examination or OCT and did not undergo US scanning. The exclusion criteria included 1) history of retinovascular disease (e.g., diabetic retinopathy and age-related macular degeneration), 2) previous ocular melanoma treatment, and 3) SS-OCTA image quality <5 or significant motion artifact impeding lesion visualization.

Baseline characteristics including age, gender, and lesion follow-up time before enrollment were recorded.

Image Acquisition

All lesions were imaged with ultra-widefield color fundus photography, B-scan US, and SS-OCTA at the time of enrollment. All SS-OCTA scanning was performed on the PLEX Elite device (Zeiss Meditec, Dublin, CA). This device works through a tunable laser of approximately 1060 nm and operates at a speed of 100,000 A-scans/sec with an A-scan depth of 3.0 mm. The 12 mm × 12 mm scan pattern was selected to increase lesion area visualization.

Image Processing

Bruch's membrane (BM) was manually segmented on all slabs to avoid segmentation errors caused by lesion elevation. Three slabs were exported per image: choriocapillaris (CC) slab, choroid slab, and lesion slab. The CC slab was defined as a 20 μm slab immediately posterior to BM, consistent with previous studies.[12–14] The choroid slab was defined as a 51 μm slab with an inner boundary 64 μm posterior to BM, as suggested by manufacturer settings. The lesion slab had an inner boundary 64 μm posterior to BM and an outer boundary 400 μm posterior to BM. This slab captured all flow pixels within the choroid. Scans underwent projection removal of overlying vasculature with built-in device software before analysis.

Image Grading

General characteristics recorded for each lesion included distance from the fovea and optic nerve

From the *Department of Ophthalmology, New England Eye Center, Tufts Medical Center, Boston, Massachusetts; †Yale School of Medicine, New Haven, Connecticut; and ‡Department of Ophthalmology, Federal University of Sao Paulo, Sao Paulo, Brazil.

Supported in part by a Massachusetts Lions Club Grant, a Research to Prevent Blindness Challenge Grant, and the Yale School of Medicine Medical Student Research Fellowship. J. S. Duker receives research support from Carl Zeiss Meditec (Jena, Germany) and Optovue Inc (Fremont, CA). He is a consultant at Allergan Pharmaceuticals (Dublin, Ireland), Aura Biosciences (Cambridge, MA), Bausch Health (Laval, Canada), Novartis (Basel, Switzerland), and Roche (Basel, Switzerland). He is a director of entity at Sesen Bio (Cambridge, Massachusetts) and an employee of EyePoint Pharma (Watertown, MA). He is a shareholder at Hemera Biosciences (Waltham, MA). N. K. Waheed is a consultant for Topcon (Tokyo, Japan), Roche/Genentech (San Francisco, California), Regeneron (Tarrytown, New York), Apellis (Waltham, Massachusetts), Astellas (Tokyo, Japan), Boehringer Ingelheim (Ingelheim, Germany), and Novartis (Basel, Germany); she is a speaker for Nidek Medical Products (Gamagori, Japan) and Topcon (Tokyo, Japan); she is an officer of entity at Gyroscope (Ambler, Pennsylvania); she has a personal financial interest in the Boston Imaging Reading Center (Boston, Massachusetts) and Ocudyne. The remaining authors have no conflicting interests to disclose.

Reprint requests: Jay S. Duker, MD, Department of Ophthalmology, Tufts Medical Center, 800 Washington Street, Box 450, Boston, MA 02111; e-mail: jduker@tuftsmedicalcenter.org

head, as well as presence of CC compression and RPE disruption. Choriocapillaris compression was determined on cross-sectional OCT, as defined in a recent publication.[15] Images were graded for high-risk multimodal imaging features outlined in previous studies, including lesion depth >2 mm, acoustic hollowness, overlying fluid, shaggy photoreceptors, greatest basal diameter >5 mm, and orange pigment.[16,17] The total number of high-risk features was tallied for each subject, with a maximum score of 6.

Although high-risk features of nevi and melanomas have been previously identified on OCT, color fundus photography, and US, the current study explored candidate vascular features on OCTA imaging. Vascular features assessed included CC signal, choroidal vessel visualization, mean choroidal vessel depth, and deepest choroidal vessel.

Choriocapillaris signal was assessed on the CC slab by examining the en face image and corresponding cross-sectional OCT with flow overlay. Choriocapillaris signal was graded as increased, decreased, or equivalent to the surrounding, unaffected CC (Figure 1). Only lesion sectors without significant shadowing because of fluid or other overlying structures were graded in this analysis, as the occurrence of shadowing precludes proper flow signal assessment. Similarly, increased CC signal was considered only in the absence of overlying RPE atrophy because atrophic changes lead to signal hyper transmission. Qualitative CC grading was selected over quantitative assessment as wide-field OCTA scans have reduced reproducibility of vessel density measures, particularly in the CC.[18]

The current study assessed the use of SS-OCTA for vessel visualization in melanomas and nevi. Vessels within these choroidal lesions were collectively referred to as choroidal vessels. This wording was selected because histologic evaluation, needed to differentiate between normal choroidal vasculature and intrinsic tumor vasculature, was not performed in this study.[3] Visible choroidal vessels were defined as hyperreflective vessels seen on en face imaging, consistent with previous studies (Figure 2).[19] Choroidal vessel visualization on choroidal and lesion slabs was assessed on a head-to-head comparison by two independent graders (ESL and LSMM). Graders were blinded to lesion and slab type during assessment.

Lesions with visible choroidal vessels underwent further assessment. Lesion slabs were used for choroidal vessel evaluation. Internal vascular pattern and the presence of avascular areas were determined for each lesion. Avascular areas were defined as regions with absent choroidal vasculature and no overlying shadowing. Choroidal vessel depth was measured on cross-sectional OCT with flow overlay. Depth was determined as the distance from BM to the first flow pixel for a given vessel (Figure 2G). If BM could not be visualized, the bottom boundary of the RPE was used as proxy. Only choroidal vessels identified on both en face and cross-sectional OCTA were measured. The depth of 5 distinct vessels was measured for each lesion, and mean choroidal vessel depth was calculated. The deepest choroidal vessel within each lesion was also recorded. The mean choroidal vessel depth and deepest choroidal vessel were further assessed as binary outcomes. Vessels in the top 75th percentile for each category received a score of 1, whereas those below the cut-off received a score of 0.

Statistical Analysis

Baseline characteristics and OCTA vascular features were compared across the lesion type using analysis of variance and chi-square tests. Significant results were further evaluated by Tukey's honest significance and post-hoc residual testing to elucidate differences on pair-wise comparison. Spearman correlation analysis was performed to assess the relationship between total number of high-risk features and vascular features identified on OCTA. To control for lesion depth, a size-matched cohort of 5 elevated nevi and 5 melanomas with comparable depth and greatest basal diameter was assessed. Student's t and Fisher's exact tests were used for comparison between these two size-controlled groups. In addition, these tests were used to determine if a relationship existed between CC compression, lesion depth, and CC flow reduction in the overall cohort.

To determine what slab was superior for choroidal vessel visualization, a head-to-head comparison of choroidal and lesion slabs was performed by two expert graders. Gradings from each reader were considered as independent measures. Interrater reliability for this comparison was assessed by Cohen's kappa.

All statistical analyses were performed on RStudio Version 1.1.463.[20]

Results

Of 35 patients recruited to this study, 29 lesions from 29 subjects were included in the final analysis. Three subjects had peripheral lesions that could not be captured on OCTA imaging, and three subjects had poor quality imaging. In total, 7 flat choroidal nevi, 17 elevated choroidal nevi, and 5 choroidal melanomas were analyzed. Demographic, baseline, and vascular features are summarized in Table 1.

Choroidal vessels were identified in 14% of flat choroidal nevi, 77% of elevated choroidal nevi, and

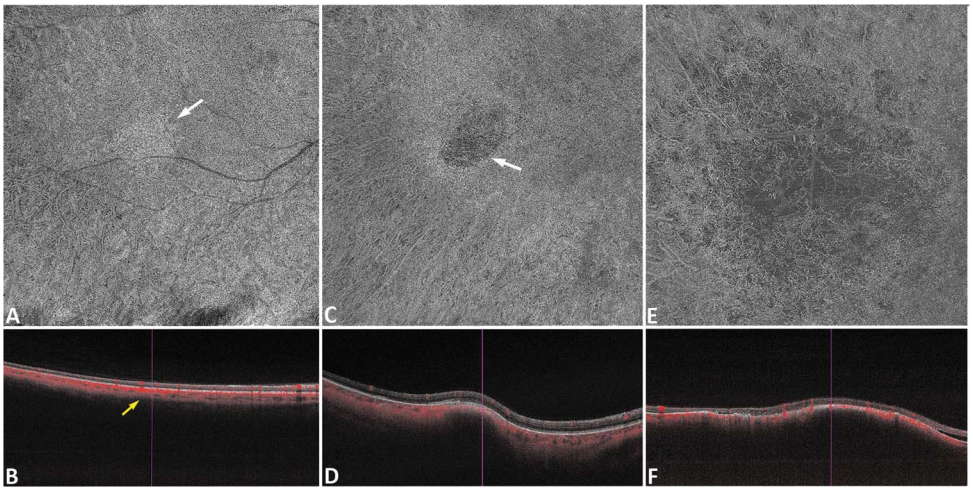

Fig. 1. Choriocapillaris flow assessment in flat choroidal nevus, elevated nevus, and melanoma. **A** and **B.** Choriocapillaris slab of a flat choroidal nevus and corresponding cross-sectional OCT with flow overlay. **A.** En face image shows increased signal over the lesion (white arrow). **B.** Cross-sectional image reveals increased choriocapillaris flow (yellow arrow). **C** and **D.** Choriocapillaris slab of an elevated choroidal nevus and corresponding cross-sectional OCT with flow overlay. **C.** En face image shows decreased signal over the lesion (white arrow). **D.** Cross-sectional image reveals decreased choriocapillaris flow. **E** and **F.** Choriocapillaris slab of a choroidal melanoma and corresponding cross-sectional OCT with flow overlay. **E.** En face image shows decreased signal over the lesion. **F.** Cross-sectional image reveals decreased choriocapillaris flow.

100% of choroidal melanomas. Of 19 lesions with visible choroidal vessels, the lesion slab was superior for choroidal vessel visualization in 90% (17) of cases. Graders agreed in 95% (18) of cases, and the Kappa coefficient of interrater reliability was 0.64 (P = 0.0036), indicating substantial agreement between graders.[21] The full-lesion slab was, therefore, selected for subsequent assessment of choroidal vasculature.

All nevi had normal choroidal vasculature with straight and parallel vessels. Vessels visualized were numerous and of a small caliber (Figure 3). Peripheral vessels were more clearly visualized than central vessels. A majority of elevated choroidal nevi (63%) had small avascular areas. Of 5 melanomas assessed, two had "nevus-like" architecture with straight, parallel vessels, small avascular areas, and clear peripheral vessels (Figure 4). One melanoma had central shadowing with straight vessels peripherally. The two remaining melanomas had choroidal vascular loss, with large avascular areas. In one lesion, central vessels formed a looping pattern (Figure 5). In the other lesion, two large vessels cross-linked centrally (Figure 6). Unlike the parallel vessels seen in nevi, the vessels in this lesion traveled in a plane perpendicular to the retinal surface (Figure 6).

The number of total high-risk features was significantly different across the three lesion types (Table 1). Several vascular features distinguished flat choroidal nevi from higher risk lesions, including the presence of avascular areas and choroidal vessel visualization. Vascular features that differentiated melanomas from both flat and elevated choroidal nevi included mean choroidal vessel depth, deepest choroidal vessel, and deepest choroidal vessel depth >75th percentile (155 μm).

On Spearman correlation analysis, decreased CC flow (rho = 0.74, $P \leq 0.0001$), choroidal vessel visualization (rho = 0.64, P = 0.0002), mean choroidal

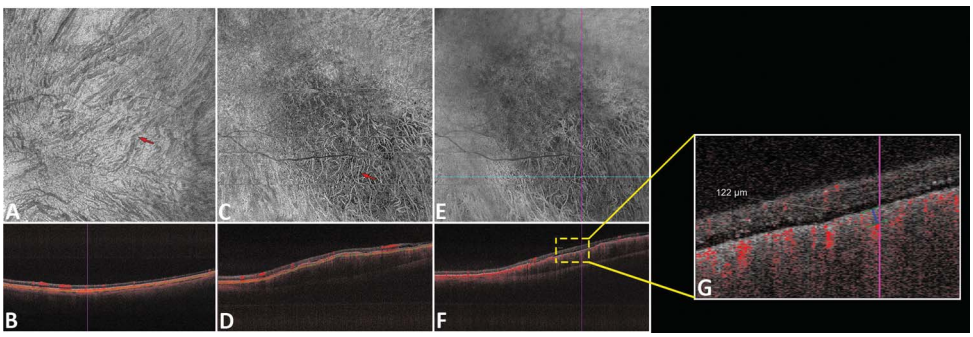

Fig. 2. Choroidal vessel visualization. **A** and **B.** Choroidal slab of a flat choroidal nevus and corresponding cross-sectional OCT with flow overlay. **A.** En face image shows dark choroidal vessels (red arrow). Such vessels were not assessed in this study as they are shadows of underlying vasculature. Only hyperreflective choroidal vessels were assessed. **C** and **D.** Choroidal slab of an elevated choroidal nevus and corresponding cross-sectional OCT with flow overlay. **C.** Red arrow shows an example of a hyperreflective choroidal vessel. **E** and **F.** Lesion slab of an elevated nevus and corresponding cross-sectional OCT with flow overlay. Choroidal vessels had to be visualized on en face and cross-sectional OCT with flow overlay to be measured. **E.** En face image shows hyperreflective choroidal vessels. Slice navigators point to a hyperreflective choroidal vessel (**F**) cross-sectional OCT with flow overlay shows vessel pixel in cross-section. **G.** Magnified cross-sectional OCT shows caliper tool and corresponding vessel depth measurement.

vessel depth (rho = 0.79, $P = 0.0001$), and deepest choroidal vessel visualized (rho = 0.80, $P = 0.0001$) were positively correlated with a total number of high-risk features. Increased CC flow was negatively correlated with a total number of high-risk features (rho = −0.41, $P = 0.026$). Separately, an association existed between CC compression and lesion depth ($t = 6.8$, $P \leq 0.0001$), as well as between CC compression and decreased CC flow (Fisher's exact, $P = 0.009$), results not shown.

To control for overall lesion depth and basal diameter, a subanalysis of size-matched elevated nevi and melanomas was performed (Table 2). In this subanalysis, mean choroidal vessel depth ($P = 0.015$), deepest choroidal vessel visualized ($P = 0.034$), and deepest choroidal vessel depth >75th percentile (155 μm) ($P = 0.048$) were significantly different across the two groups. The mean choroidal vessel depth >75th percentile (107 μm) did not vary significantly between the 2 groups.

Discussion

Pathologic studies suggest a vascular spectrum exists between choroidal nevi and melanomas.[4] Invivo visualization of this spectrum could elucidate differences between choroidal nevi and melanomas and could help identify new high-risk vascular features. This study shows that SS-OCTA can visualize distinct vascular differences between choroidal nevi and melanomas, that such differences are associated with known risk factors, and that deep choroidal vessels are more common in choroidal melanomas, even when compared with size-matched elevated choroidal nevi.

Qualitative analysis uncovered distinct vascular patterns in flat choroidal nevi, elevated choroidal nevi, and choroidal melanomas. Previous studies considered nevi in aggregate, obscuring angiographic differences between flat and elevated nevi, and exaggerating differences between high-risk nevi and choroidal melanomas. The current study analyzed each subset individually, highlighting differences between each. For instance, flat choroidal nevi had no avascular areas compared with 62.5% of elevated nevi and 100% of choroidal melanomas. Linear regression analysis showed a positive correlation between avascular areas and increasing number of high-risk features. Previous studies quote avascular area rates of 17% in choroidal nevi, suggesting their presence could help differentiate between nevi and choroidal melanomas.[22] Our more granular analysis shows that although avascular areas are more common in higher risk lesions, the presence of avascular areas may not distinguish between elevated nevi and choroidal melanomas. This is further supported by our subanalysis, which showed no differences in the presence of avascular areas between size-matched elevated choroidal nevi and choroidal melanomas.

Flat choroidal nevi were less likely to have decreased CC flow when compared with choroidal melanomas. However, there was no significant difference in CC flow reduction between elevated choroidal nevi and choroidal melanomas. These findings are consistent with previous studies describing CC thinning over these lesions and a recent study that linked CC compression to increasing choroidal nevus depth.[5,15,23–25] In the current cohort, CC compression was associated with increased lesion depth ($P \leq 0.0001$) and decreased CC flow ($P = 0.009$). It is likely, therefore, that the observed reduction in CC flow is not because of structural loss of the CC in these lesions, but to vascular congestion secondary to compression. Such vascular congestion could result in blood flow speeds below the OCTA device's detection threshold, mimicking CC loss. Interestingly, although there was a significant difference in CC compression between flat choroidal nevi and elevated choroidal nevi, no difference in CC flow reduction was observed between these two groups. This suggests that a critical amount of compression might be needed to slow CC flow speeds below the device's detection threshold. Reduced CC flow was strongly associated with increasing total risk factors in this cohort. However, no difference in CC flow existed between elevated choroidal nevi and choroidal melanomas, suggesting CC flow reduction is likely attributable to compression secondary to lesion depth rather than malignant potential.

The visualization of choroidal vessels differed across lesion types. Choroidal vessel visualization was common among elevated nevi and melanomas, but not among flat choroidal nevi. We hypothesize this is likely linked to reduced CC flow and RPE loss over nevi and melanomas.[25,26] In the current cohort, CC compression and RPE disruption were common among elevated choroidal nevi and choroidal melanomas. An intact CC network causes increased signal scattering, reducing the signal to noise ratio in underlying vascular tissues. Loss of normal CC architecture reduces scattering and increases the signal to noise ratio in the choroid, improving choroidal vessel visualization. Concomitantly, RPE loss allows for increased signal penetration into the choroid and improved choroidal vessel visualization, akin to choroidal vessel identification below areas of atrophy in dry macular degeneration.[19]

Overall, choroidal melanoma vessels were deeper than choroidal nevi vessels. Deeper vessels were seen in deeper lesions. Mean choroidal vessel depth and

Table 1. Demographic and Baseline Characteristics

Characteristic	Total (n = 29) Mean (SD)	Flat Choroidal Nevus (n = 7) Mean (SD)	Elevated Choroidal Nevus (n = 17) Mean (SD)	Choroidal Melanoma (n = 5) Mean (SD)	χ^2/F	DF	*P*	Pairwise Comparison		
								Flat vs. Elevated Choroidal Nevus (*P*)	Flat Choroidal Nevus vs. Melanoma (*P*)	Elevated Choroidal Nevus vs. Melanoma (*P*)
General features										
Age (years)	65.2 (21.3)	66.6 (17.3)	65.2 (11.8)	64.8 (6.1)	0.039	2, 26	0.96	0.97	0.96	0.99
Female	48.3%	42.9%	52.9%	40%	0.38	2	0.83	1	1	1
Follow-up (years)	7.9 (5.5)	7.3 (3.3)	8.2 (5.8)	7.4 (7.7)	0.92	2, 26	0.92	0.93	0.98	0.96
Largest basal diameter (mm)	4.4 (2.8)	1.8 (0.5)	4.3 (2.7)	7.6 (0.93)	10.2	2, 26	0.0006*	0.032*	0.0004*	0.024*
Lesion depth (mm)	2.7 (1.3)	—	1.85 (1)	3.3 (0.6)	23.3	2, 26	<0.0001*	0.0004*	<0.0001*	0.0016*
Distance from fovea (mm)	2.7 (2.1)	3.8 (2.1)	2.1 (2.1)	3.0 (1.4)	1.8	2, 26	0.19	0.17	0.77	0.68
Distance from optic nerve head (mm)	3.4 (2.0)	3.3 (2.4)	3.7 (1.9)	2.6 (1.9)	0.57	2, 26	0.58	0.93	0.80	0.55
RPE disruption	48.3%	0%	58.8%	80%	9.3	2	0.009*	0.028*	0.028*	0.613
Choriocapillaris compression	58.6%	0%	70.6%	100%	14.5	2	0.0007*	0.007*	0.004*	0.29
Total high-risk features	2.2 (2.4)	0 (0)	2 (1.9)	5.8 (0.4)	21.9	2, 26	<0.0001*	0.017*	<0.0001*	0.0001*
Vascular features										
Increased choriocapillaris flow	27.6%	42.9%	29.4%	0%	2.8	2	0.25	0.66	0.43	0.43
Decreased choriocapillaris flow	55.2%	28.6%	52.9%	100%	6.1	2	0.047*	0.39	0.029*	0.17
Avascular area	53.8%	0%	62.5%	100%	10.9	2	0.0043*	0.023*	0.014*	0.27
Choroidal vessels visualized	65.5%	14.3%	76.5%	100%	11.7	2	0.003*	0.023*	0.023*	0.54
Mean choroidal vessel depth (μm)	93.1 (20.2)	70 (5.2)	84.4 (16.4)	110.1 (11.4)	6.9	2, 16	0.009*	0.21	0.011*	0.042*
Mean choroidal vessel depth >107 μm	13.8%	0%	5.9%	60%	14.2	2	0.0008*	1	0.036*	0.035*
Deepest choroidal vessel (μm)	122.2 (43.9)	74.4 (9.3)	110 (31.9)	180.3 (28.7)	9.3	2, 16	0.0024*	0.45	0.017*	0.004*
Deepest choroidal vessel >155 μm	17.2%	0%	5.9%	100%	21.6	2	<0.0001*	1	0.0045*	0.0025*

*Statistically significant ($P < 0.05$).
χ^2, chi-square statistic; DF, degrees of freedom; F, F statistic (ANOVA test).

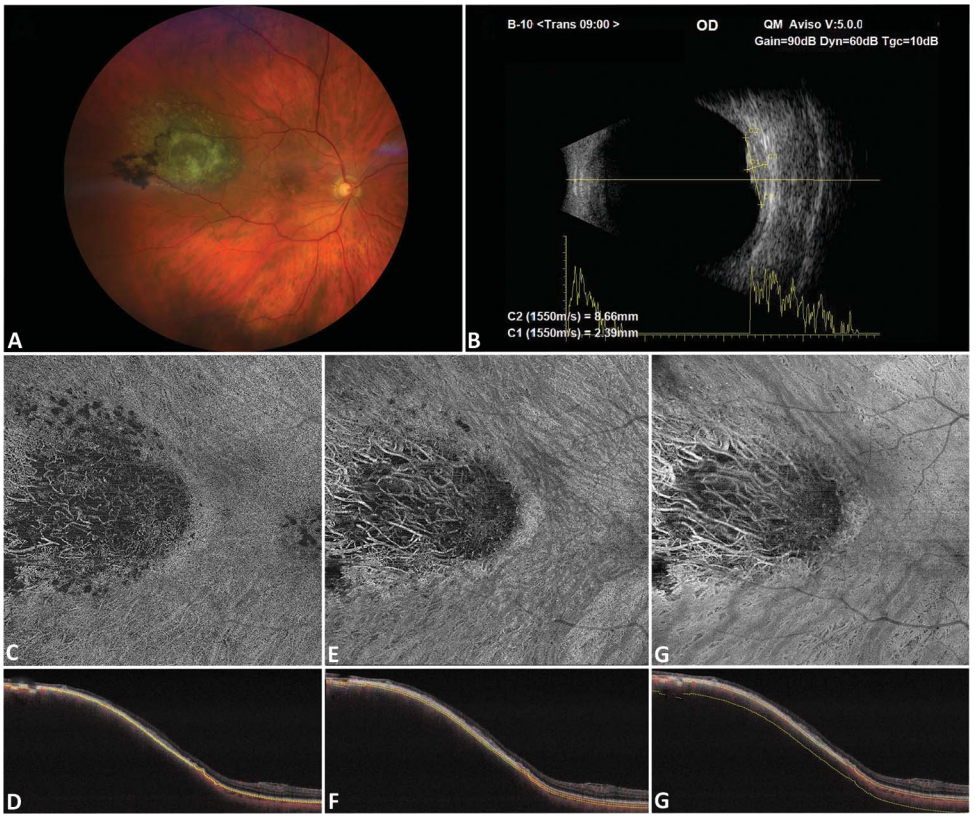

Fig. 3. Elevated choroidal nevus. **A.** Color fundus photograph of an elevated choroidal nevus. **B.** B-scan US of an elevated choroidal nevus, depth 2.39 mm. **C** and **D.** Choriocapillaris slab of an elevated choroidal nevus and corresponding cross-sectional OCT with flow overlay. Reduced CC flow is noted on en face and cross-section. **E** and **F.** Choroidal slab of an elevated choroidal nevus and corresponding cross-sectional OCT with flow overlay. Avascular areas are noted throughout the lesion with increased spacing between adjacent vessels. **G** and **H.** Lesion slab of an elevated choroidal nevus and corresponding cross-sectional OCT with flow overlay. Choroidal vessels visualized are straight and parallel in nature. Areas of central shadowing are noted.

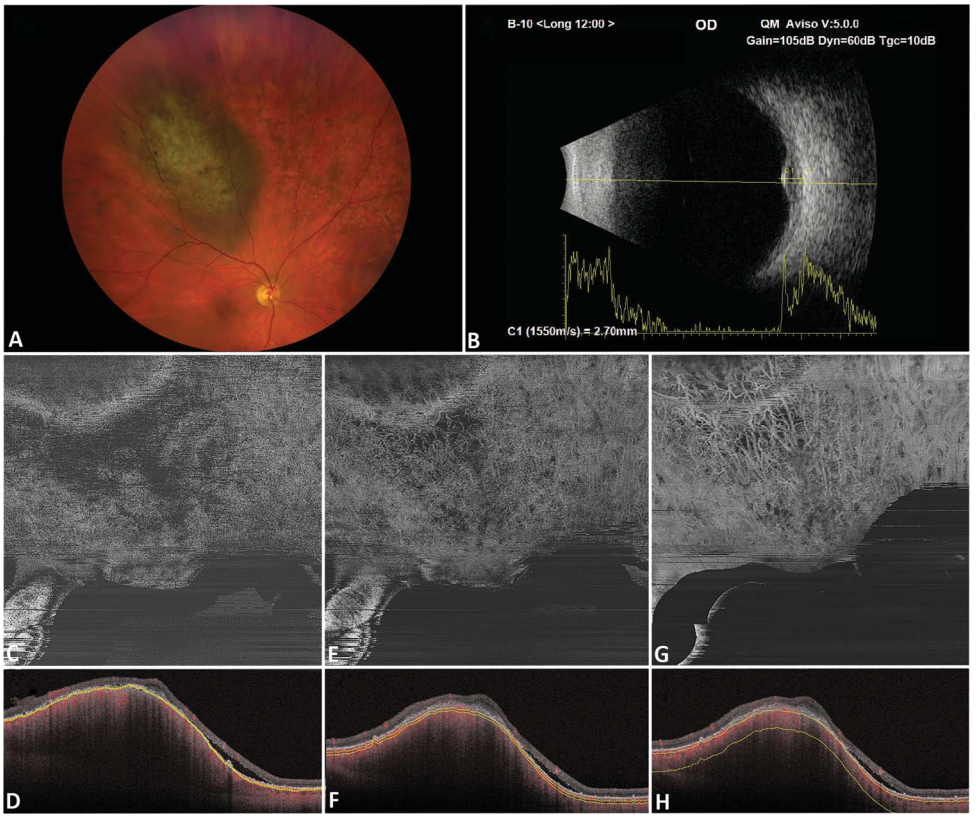

Fig. 4. Choroidal melanoma with nevus-like architecture. **A.** Color fundus photograph of a choroidal melanoma. **B.** B-scan US of a choroidal melanoma, depth 2.70 mm. **C** and **D.** Choriocapillaris slab of a choroidal melanoma and corresponding cross-sectional OCT with flow overlay. Reduced CC flow is notable on en face and cross-section. Significant shadowing impedes proper assessment superiorly. **E** and **F.** Choroid slab of a choroidal melanoma and corresponding cross-sectional OCT with flow overlay. Avascular areas are noted superiorly. **G** and **H.** Lesion slab of a choroidal melanoma and corresponding cross-sectional OCT with flow overlay. Choroidal vessels appear straight and parallel in nature. No looping or cross-linking is noted, vessels travel parallel to the retinal surface. Areas of avascularity distance neighboring vessels.

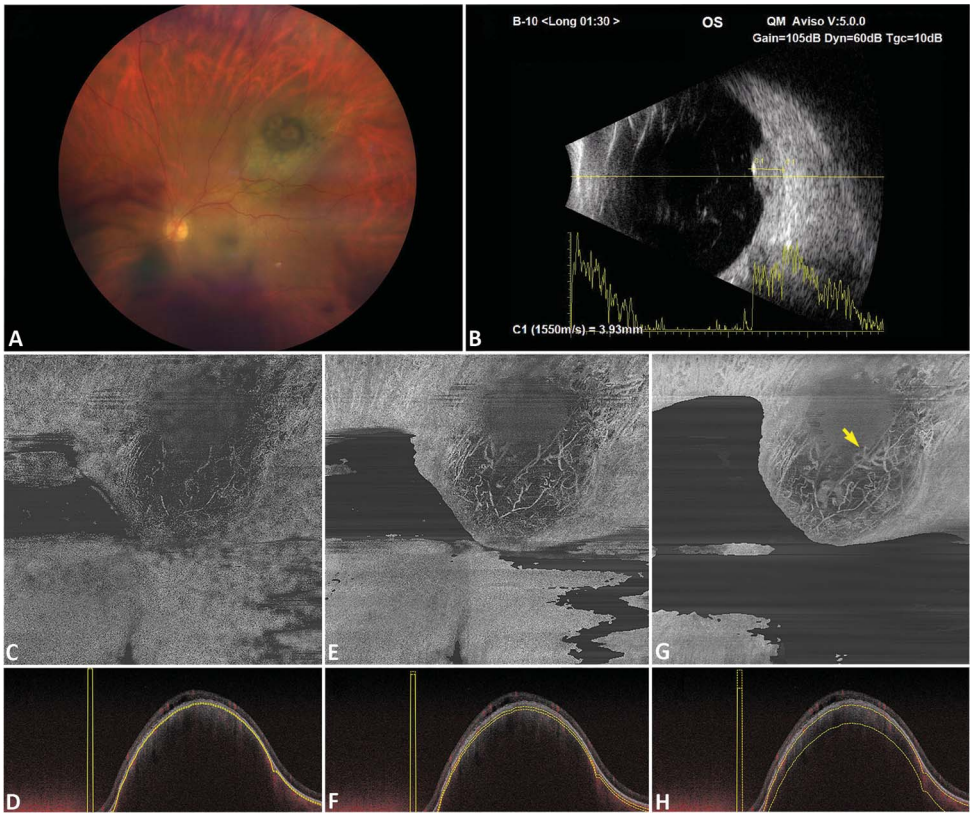

Fig. 5. Choroidal melanoma with vessel loops. **A.** Color fundus photograph of a choroidal melanoma. **B.** B-scan US of a choroidal melanoma, depth 3.93 mm. **C** and **D.** Choriocapillaris slab of a choroidal melanoma and corresponding cross-sectional OCT with flow overlay. Reduced CC flow centrally is noted on both images. There is significant shadowing superiorly as the tumor extends beyond the imaging frame in this area. **E** and **F.** Choroid slab of a choroidal melanoma and corresponding cross-sectional OCT with flow overlay. Areas of avascularity are noted centrally and inferiorly. **G** and **H.** Lesion slab of a choroidal melanoma and corresponding cross-sectional OCT with flow overlay. **G.** Superficially, distorted choroidal vessels of small caliber are noted (white arrowhead). Deeper vessels of greater caliber with multiple loops are noted centrally (yellow arrow).

deepest choroidal vessel visualized were successively greater for flat nevi, elevated nevi, and melanomas, suggesting a positive relationship between a lesion's depth and the depth of choroidal vasculature visualized. However, even after controlling for lesion depth and greatest basal diameter in our size-matched subanalysis, mean choroidal vessel depth, deepest choroidal vessel visualized, and deepest choroidal vessel >155 μm were significantly greater for melanomas than similarly sized elevated nevi. In healthy eyes, the choroid is a dense vascular structure. As cancerous cells replicate, they can compress and occlude vessels,

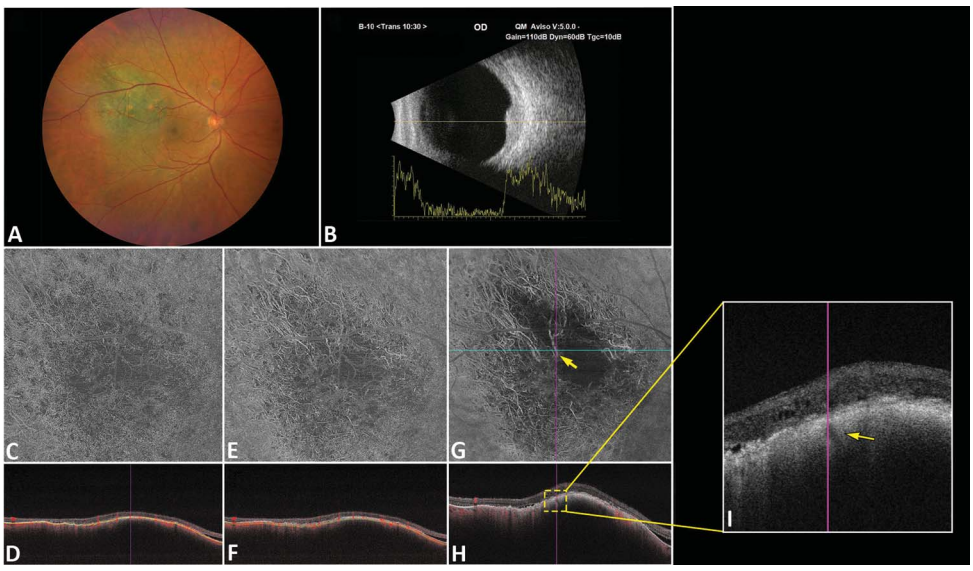

Fig. 6. Choroidal melanoma with vessel cross-linking. **A.** Color fundus photograph of a choroidal melanoma. **B.** B-scan US of a choroidal melanoma, depth 3.94 mm. **C** and **D.** Choriocapillaris slab of a choroidal melanoma and corresponding cross-sectional OCT with flow overlay. Reduced CC flow centrally is noted on both images. **E** and **F.** Choroidal slab of a choroidal melanoma and corresponding cross-sectional OCT with flow overlay. A large, avascular area is noted centrally. **G** and **H.** Lesion slab of a choroidal melanoma and corresponding cross-sectional OCT with flow overlay. **G.** There are few choroidal vessels centrally, with more choroidal vasculature noted toward the lesion's periphery. **G.** Two large vessels arise within the lesion and appear to cross-link centrally (yellow arrow). **H.** Cross-sectional OCT with flow overlay. **I.** Magnified cross-sectional OCT shows vessel traveling perpendicular to the retinal surface (yellow arrow).

Table 2. Size-Matched Subanalysis

Characteristic	Elevated Choroidal Nevus (n = 5) Mean (SD)	Choroidal Melanoma (n = 5) Mean (SD)	*t*-value	*P*
General features				
Age (years)	58 (17.4)	64.8 (6.1)	0.82	0.43
Female	60%	40%	—	1
Follow-up (years)	6.2 (5.0)	7.4 (7.7)	0.29	0.78
Largest basal diameter (mm)	6.50 (0.83)	7.6 (0.93)	1.99	0.10
Lesion depth (mm)	2.70 (0.37)	3.3 (0.6)	1.7	0.12
Distance from the fovea (mm)	1.93 (1.0)	3.0 (1.4)	1.30	0.23
Distance from ONH (mm)	3.9 (2.1)	2.6 (1.9)	1.1	0.31
RPE disruption	80%	80%	—	1
Choriocapillaris compression	100%	100%	—	1
Total high-risk features	3.6 (1.14)	5.8 (0.4)	5.37	0.0007*
Vascular features				
Increased choriocapillaris flow	20%	0%	—	1
Decreased choriocapillaris flow	80%	100%	—	1
Avascular area	80%	100%	—	1
Choroidal vessels visualized	80%	100%	—	1
Mean choroidal vessel depth (μm)	90.58 (26.32)	110.1 (11.4)	2.0	0.015*
Mean choroidal vessel depth >107 μm	29%	60%	—	0.21
Deepest choroidal vessel (μm)	125.4 (32.87)	180.3 (28.7)	2.6	0.034*
Deepest choroidal vessel >155 μm	20%	100%	—	0.048*

*Statistically significant ($P < 0.05$).

ultimately leading to known ischemic changes, such as such as RPE degeneration, serous retinal detachments, and cystic retinal degeneration.[27,28] Breakdown of the normal choroidal architecture allows for increased signal penetration and improved visualization of deeper vessels in malignant lesions. Findings from the overall and size-matched cohort suggest that choroidal vessel depth measures could identify high-risk lesions independent of lesion depth and could be of interest for tracking lesion growth. Given the small sample size of the current study, however, larger studies assessing greater numbers of choroidal melanomas are needed to appropriately control for the lesion size.

Differences in vessel morphology were appreciated between nevi and a subset of melanomas. All nevi displayed parallel vessels, similar to normal choroidal vasculature seen on prototype OCTA images.[29] We identified two types of vasculature within our melanoma cohort: "nevus-like" vasculature and complex vasculature. Melanomas with "nevus-like" vasculature had straight, parallel vessels, whereas those with complex vasculature showed vascular looping and cross-linking. Pathologic studies have postulated that disorganized vessel patterns arise in high-risk tumors where rapidly replicating cells compromise normal choroidal perfusion, resulting in ischemia and subsequent angiogenesis.[28] Although the vascular patterns visualized in this study match tumor vessel patterns previously described in histologic studies, the imaged lesions did not undergo resection.[28] Thus, there is no way to determine if the vessel patterns seen on SS-OCTA in fact correlate with those described in histopathologic studies. It is nevertheless promising that distinct vascular patterns can be appreciated across different lesion types on swept-source imaging.

Overall, normal choroidal vasculature and straight, parallel vessels were more common in benign lesions, and less common in their malignant counterparts, consistent with histologic findings.[28] Rummelt et al described the existence of two choroidal melanoma subtypes, those with malignant vasculature, and those with "nevus-like" vasculature. Melanomas with malignant vasculature were more likely to metastasize.[4] As described above, the current study identified two similar melanoma subtypes on SS-OCTA imaging. Longitudinal studies with larger sample sizes and genetic profiling are needed to determine whether prognosis differs between lesions with nevus-like and complex vasculature as identified on OCTA. If so, SS-OCTA could facilitate invivo assessment of tumor prognosis, something not currently available through high-risk feature evaluation alone.[30]

There are several limitations to this study. First, although SS-OCTA has improved penetration into the choroid, in most cases, only a fraction of the lesion depth was visualized. Thus, identified differences are

based solely on vessels residing within the first 400 μm of each lesion. Second, the cross-sectional nature of this study limited its diagnostic reliability. Although most subjects had been clinically followed for years before enrollment, four subjects were enrolled at the first clinical encounter. A lesion diagnosed as a nevus on initial evaluation might be diagnosed as a melanoma on follow-up. Finally, and most importantly, only 5 treatment-naïve choroidal melanomas were assessed in this study, and genetic data were not obtained for these cases. The small sample size of this study limited our ability to control for lesion depth, an important confounder in this analysis. Although a subanalysis of size-matched elevated nevi and choroidal melanoma showed encouraging results, larger scale studies that thoroughly control for lesion depth and diameter are needed to determine if choroidal vessel depth is an independent risk factor when assessing these lesions.

Despite these limitations, the current study captured morphologic differences between treatment-naïve choroidal melanomas, elevated choroidal nevi and flat choroidal nevi, and identified potential vascular risk factors within these lesions. Mean choroidal vessel depth, deepest choroidal vessel, and the presence of a deep choroidal vessel >155 μm were greater among choroidal melanomas than similarly sized elevated nevi. Furthermore, SS-OCTA imaging captured clear vascular patterns within choroidal nevi and small choroidal melanomas. Although OCTA features may not supplant preestablished risk factors, vascular markers found in the current study could provide additional information for the assessment of challenging cases.

Key words: choroidal melanoma, choroidal nevi, swept-source optical coherence tomography angiography.

References

1. Shields CL, Furuta M, Thangappan A, et al. Metastasis of uveal melanoma millimeter-by-millimeter in 8033 consecutive eyes. Arch Ophthalmol 2009;127:989–998.
2. Gass JD. Problems in the differential diagnosis of choroidal nevi and malignant melanoma. XXXIII Edward Jackson Memorial lecture. Am J Ophthalmol 1977;83:19–48.
3. Folberg R, Mehaffey M, Gardner LM, et al. The microcirculation of choroidal and ciliary body melanomas. Eye (Lond) 1997;11:227–238.
4. Rummelt V, Folberg R, Rummelt C, et al. Microcirculation architecture of melanocytic nevi and malignant melanomas of the ciliary body and choroid. A comparative histopathologic and ultrastructural study. Ophthalmology 1994;101:718–727.
5. Ghassemi F, Mirshahi R, Fadakar K, Sabour S. Optical coherence tomography angiography in choroidal melanoma and nevus. Clin Ophthalmol 2018;12:207–214.
6. Toledo JJ, Asencio-Duran M, García-Martinez JR, López-Gaona A. Use of OCT angiography in choroidal melanocytic tumors. J Ophthalmol 2017;2017:1573154.
7. Cennamo G, Romano MR, Breve MA, et al. Evaluation of choroidal tumors with optical coherence tomography: enhanced depth imaging and OCT-angiography features. Eye (Lond) 2017;31:906–915.
8. Spaide RF, Fujimoto JG, Waheed NK, et al. Optical coherence tomography angiography. Prog Retin Eye Res 2018;64:1–55.
9. Ferenczy SR, Shields CL. Optical coherence tomography angiography: an overview of applications in ocular oncology. J Ophthalmic Photography 2018;40:70–78.
10. Ali ZC, Gray J, Balaskas K. Features of choroidal naevi on swept source optical coherence tomography angiography and structural reverse flow optical coherence tomography. Graefes Arch Clin Exp Ophthalmol 2018;256:1319–1323.
11. Pellegrini M, Corvi F, Invernizzi A, et al. Swept-source optical coherence tomography angiography IN choroidal melanoma: an analysis of 22 consecutive cases. Retina 2019;39:1510–1519.
12. Braun PX, Mehta N, Gendelman I, et al. Global analysis of macular choriocapillaris perfusion in dry age-related macular degeneration using swept-source optical coherence tomography angiography. Invest Ophthalmol Vis Sci 2019;60:4985–4990.
13. Zhang Q, Zheng F, Motulsky EH, et al. A novel strategy for quantifying choriocapillaris flow voids using swept-source OCT angiography. Invest Ophthalmol Vis Sci 2018;59:203–211.
14. Thulliez M, Zhang Q, Shi Y, et al. Correlations between choriocapillaris flow deficits around geographic atrophy and enlargement rates based on swept-source OCT imaging. Ophthalmol Retina 2019;3:478–488.
15. Yu MD, Dalvin LA, Ancona-Lezama D, et al. Choriocapillaris compression correlates with choroidal nevus-associated subretinal fluid: OCT analysis of 3431 cases. Ophthalmology 2020; 127:1273–1276.
16. Shields CL, Kaliki S, Rojanaporn D, et al. Enhanced depth imaging optical coherence tomography of small choroidal melanoma: comparison with choroidal nevus. Arch Ophthalmol 2012;130:850–856.
17. Shields CL, Dalvin LA, Ancona-Lezama D, et al. Choroidal nevus imaging features IN 3,806 cases and risk factors for transformation into melanoma in 2,355 cases: the 2020 taylor R. Smith and victor T. Curtin lecture. Retina 2019;39:1840–1851.
18. Rabiolo A, Gelormini F, Marchese A, et al. Macular perfusion parameters in different angiocube sizes: does the size matter in quantitative optical coherence tomography angiography? Invest Ophthalmol Vis Sci 2018;59:231–237.
19. Diaz JD, Wang JC, Oellers P, et al. Imaging the deep choroidal vasculature using spectral domain and swept source optical coherence tomography angiography. J Vitreoretin Dis 2018;2:146–154.
20. R: A Language and Environment for Statistical Computing [computer Program]. Vienna, Austria: R Foundation for Statistical Computing; 2012.
21. Landis JR, Koch GG. The measurement of observer agreement for categorical data. Biometrics 1977;33:159–174.
22. Garcia-Arumi Fuste C, Peralta Iturburu F, Garcia-Arumi J. Is optical coherence tomography angiography helpful in the differential diagnosis of choroidal nevus versus melanoma? Eur J Ophthalmol 2020;30:723–729.
23. Shah SU, Kaliki S, Shields CL, et al. Enhanced depth imaging optical coherence tomography of choroidal nevus in 104 cases. Ophthalmology 2012;119:1066–1072.
24. Filloy A, Caminal JM, Arias L, et al. Swept source optical coherence tomography imaging of a series of choroidal tumours. Can J Ophthalmol 2015;50:242–248.
25. Damato BE, Foulds WS. Tumour-associated retinal pigment epitheliopathy. Eye (Lond) 1990;4:382–387.

26. Shields CL, Furuta M, Mashayekhi A, et al. Clinical spectrum of choroidal nevi based on age at presentation in 3422 consecutive eyes. Ophthalmology 2008;115:546–552.e542.
27. Federman JL. The fenestrations of the choriocapillaris in the presence of choroidal melanoma. Trans Am Ophthalmol Soc 1982;80:498–516.
28. Folberg R, Pe'er J, Gruman LM, et al. The morphologic characteristics of tumor blood vessels as a marker of tumor progression in primary human uveal melanoma: a matched case-control study. Hum Pathol 1992;23:1298–1305.
29. Poddar R, Migacz JV, Schwartz DM, et al. Challenges and advantages in wide-field optical coherence tomography angiography imaging of the human retinal and choroidal vasculature at 1.7-MHz A-scan rate. J Biomed Opt 2017;22:1–14.
30. Jouhi S, Jager MJ, de Geus SJR, et al. The small fatal choroidal melanoma study. A survey by the European ophthalmic oncology group. Am J Ophthalmol 2019;202:100–108.